Technical design report for the PANDA endcap disc DIRC

Datar, V.; Jha, V.; Kumawat, H.; Mohanty, A. K.; Parmar, A.; Rai, A. K.; Roy, B.; Sonika, G.; Fritzsch, C.; Grieser, S.; Hergemoller, A. K.; Hetz, B.; Husken, N.; Khoukaz, A.; Wessels, J. P.; Herold, C.; Khosonthongkee, K.; Kobdaj, C.; Limphirat, A.; Srisawad, P.; Yan, Y.; Blinov, A. E.; Kononov, S.; Kravchenko, E. A.; Antokhin, E.; Barnyakov, M.; Barnyakov, A. Y.; Beloborodov, K.; Blinov, V. E.; Bobrovnikov, V. S.; Kuyanov, I. A.; Onuchin, A. P.; Pivovarov, S.; Pyata, E.; Serednyakov, S.; Tikhonov, Y.; Kunne, R.; Marchand, D.; Ramstein, B.; van de Wiele, J.; Wang, Y.; Boca, G.; Burian, V.; Finger, M.; Finger, M.; Nikolovova, A.; Pesek, M.; Peskova, M.; Pfeffer, M.; Prochazka, I.; Slunecka, M.; Gallus, P.; Jary, V.; Novy, J.; Tomasek, M.; Virius, M.; Vrba, V.; Abramov, V.; Belikov, N.; Bukreeva, S.; Davidenko, A.; Derevschikov, A.; Goncharenko, Y.; Grishin, V.; Kachanov, V.; Kormilitsin, V.; Levin, A.; Melnik, Y.; Minaev, N.; Mochalov, V.; Morozov, D.; Nogach, L.; Poslavskiy, S.; Ryazantsev, A.; Ryzhikov, S.; Semenov, P.; Shein, I.; Uzunian, A.; Vasiliev, A.; Yakutin, A.; Roy, U.; Yabsley, B.; Belostotski, S.; Gavrilov, G.; Izotov, A.; Manaenkov, S.; Miklukho, O.; Veretennikov, D.; Zhdanov, A.; Back, T.; Cederwall, B.; Makonyi, K.; Preston, M.; Tegner, P. E.; Wolbing, D.; Godre, S.; Bussa, M. P.; Marcello, S.; Spataro, S.; Iazzi, F.; Introzzi, R.; Lavagno, A.; Calvo, D.; De Remigis, P.; Filippi, A.; Mazza, G.; Rivetti, A.; Wheadon, R.; Martin, A.; Calen, H.; Ikegami Andersson, W.; Johansson, T.; Kupsc, A.; Marciniewski, P.; Papenbrock, M.; Pettersson, J.; Regina, J.; Schonning, K.; Wolke, M.; Diaz, J.; Pothodi Chackara, V.; Chlopik, A.; Kesik, G.; Melnychuk, D.; Slowinski, B.; Trzcinski, A.; Wojciechowski, M.; Wronka, S.; Zwieglinski, B.; Buhler, P.; Marton, J.; Steinschaden, D.; Suzuki, K.; Widmann, E.; Zimmermann, S.; Zmeskal, J.. - In: JOURNAL OF PHYSICS. G, NUCLEAR AND PARTICLE PHYSICS. - ISSN 0954-3899. - STAMPA. - 49:120501(2022), pp. 120501-1-120501-129. [10.1088/1361-6471/abb6c1]

Technical Design Report for the $\overline{\text{P}}$ANDA Endcap Disc DIRC

(AntiProton Annihilations at Darmstadt)

Strong Interaction Studies with Antiprotons

$\overline{\text{P}}$ANDA Collaboration

January, 2020

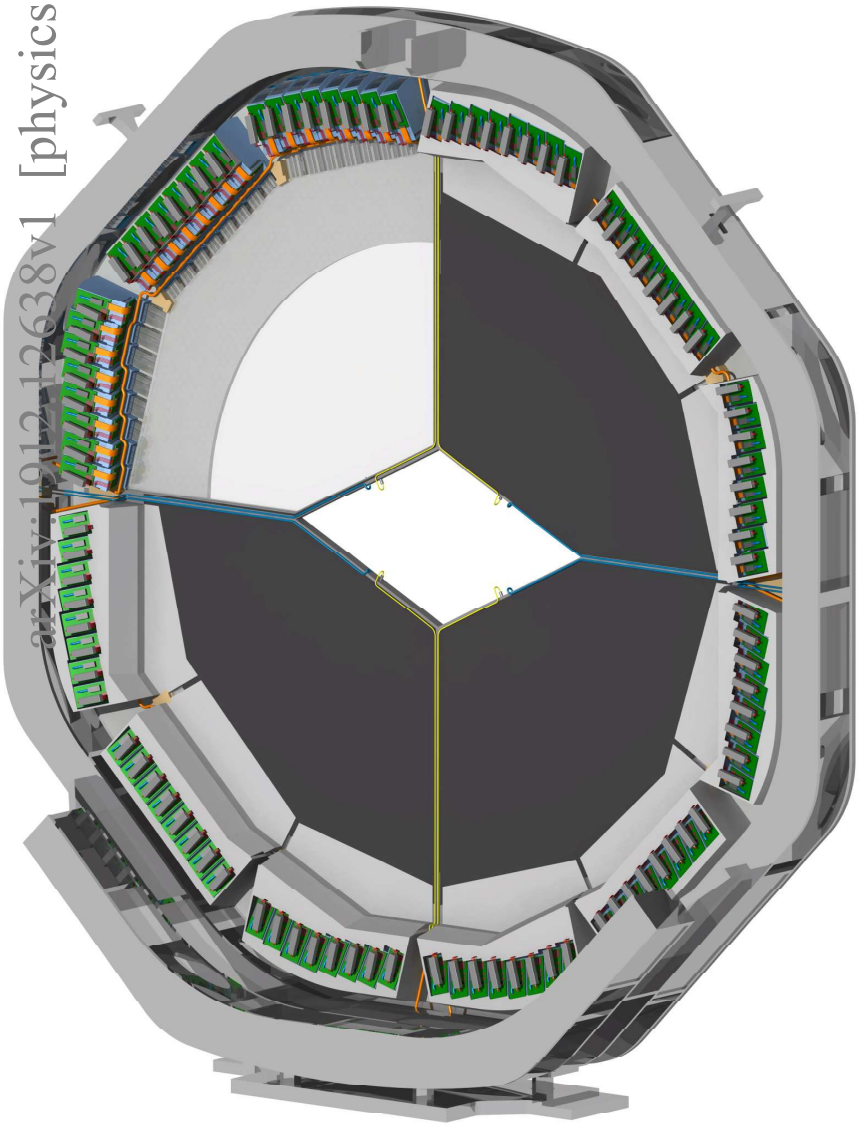

The $\overline{P}$ANDA Collaboration

Università Politecnica delle Marche-Ancona, **Ancona**, Italy
F. Davì

Universität Basel, **Basel**, Switzerland
W. Erni, B. Krusche, M. Steinacher, N. Walford

Institute of High Energy Physics, Chinese Academy of Sciences, **Beijing**, China
H. Liu, Z. Liu, B. Liu, X. Shen, C. Wang, J. Zhao

Ruhr-Universität Bochum, Institut für Experimentalphysik I, **Bochum**, Germany
M. Albrecht, T. Erlen, F. Feldbauer, M. Fink, V. Freudenreich, M. Fritsch, F.H. Heinsius, T. Held, T. Holtmann, I. Keshk, H. Koch, B. Kopf, M. Kuhlmann, M. Kümmel, S. Leiber, P. Musiol, A. Mustafa, M. Pelizäus, A. Pitka, G. Reicherz, M. Richter, C. Schnier, T. Schröder, S. Sersin, L. Sohl, C. Sowa, M. Steinke, T. Triffterer, U. Wiedner

Rheinische Friedrich-Wilhelms-Universität Bonn, **Bonn**, Germany
R. Beck, C. Hammann, J. Hartmann, B. Ketzer, M. Kube, M. Rossbach, C. Schmidt, R. Schmitz, U. Thoma, M. Urban

Università di Brescia, **Brescia**, Italy
A. Bianconi

Institutul National de C&D pentru Fizica si Inginerie Nucleara "Horia Hulubei", **Bukarest-Magurele**, Romania
M. Bragadireanu, D. Pantea

University of Technology, Institute of Applied Informatics, **Cracow**, Poland
W. Czyzycki, M. Domagala, G. Filo, J. Jaworowski, M. Krawczyk, E. Lisowski, F. Lisowski, M. Michałek, J. Płażek

IFJ, Institute of Nuclear Physics PAN, **Cracow**, Poland
K. Korcyl, A. Kozela, P. Kulessa, P. Lebiedowicz, K. Pysz, W. Schäfer, A. Szczurek

AGH, University of Science and Technology, **Cracow**, Poland
T. Fiutowski, M. Idzik, B. Mindur, K. Swientek

Instytut Fizyki, Uniwersytet Jagiellonski, **Cracow**, Poland
J. Biernat, B. Kamys, S. Kistryn, G. Korcyl, W. Krzemien, A. Magiera, P. Moskal, W. Przygoda, Z. Rudy, P. Salabura, J. Smyrski, P. Strzempek, A. Wronska

FAIR, Facility for Antiproton and Ion Research in Europe, **Darmstadt**, Germany
I. Augustin, R. Böhm, I. Lehmann, D. Nicmorus Marinescu, L. Schmitt, V. Varentsov

GSI Helmholtzzentrum für Schwerionenforschung GmbH, **Darmstadt**, Germany
M. Al-Turany, A. Belias, H. Deppe, N. Divani Veis, R. Dzhygadlo, H. Flemming, A. Gerhardt, K. Götzen, R. Karabowicz, U. Kurilla, D. Lehmann, S. Löchner, J. Lühning, U. Lynen, S. Nakhoul, H. Orth, K. Peters, T. Saito, G. Schepers, C. J. Schmidt, C. Schwarz, J. Schwiening, A. Täschner, M. Traxler, B. Voss, P. Wieczorek, A. Wilms

Joint Institute for Nuclear Research, **Dubna**, Russia
V. Abazov, G. Alexeev, V. A. Arefiev, V. Astakhov, M. Yu. Barabanov, B. V. Batyunya, V. Kh. Dodokhov, A. Efremov, A. Fechtchenko, A. Galoyan, G. Golovanov, E. K. Koshurnikov, Y. Yu. Lobanov, V. I. Lobanov, V. Malyshev, A. G. Olshevskiy, A. A. Piskun, A. Samartsev, M. G. Sapozhnikov, N. B. Skachkov, A. N. Skachkova, E. A. Strokovsky, V. Tokmenin, V. Uzhinsky, A. Verkheev, A. Vodopianov, N. I. Zhuravlev, A. Zinchenko

University of Edinburgh, **Edinburgh**, United Kingdom
D. Branford, D. Glazier, D. Watts

Friedrich Alexander Universität Erlangen-Nürnberg, **Erlangen**, Germany
M. Böhm, W. Eyrich, A. Lehmann, D. Miehling, M. Pfaffinger, S. Stelter, F. Uhlig

Northwestern University, **Evanston**, U.S.A.
S. Dobbs, K. Seth, A. Tomaradze, T. Xiao

Università di Ferrara and INFN Sezione di Ferrara, **Ferrara**, Italy
D. Bettoni

Goethe Universität, Institut für Kernphysik, **Frankfurt**, Germany
A. Ali, A. Hamdi, M. Krebs, F. Nerling

Frankfurt Institute for Advanced Studies, **Frankfurt**, Germany
V. Akishina, S. Gorbunov, I. Kisel, G. Kozlov, M. Pugach, M. Zyzak

INFN Laboratori Nazionali di Frascati, **Frascati**, Italy
N. Bianchi, P. Gianotti, C. Guaraldo, V. Lucherini

Dept of Physics, University of Genova and INFN-Genova, **Genova**, Italy
G. Bracco

Justus Liebig-Universität Gießen II. Physikalisches Institut, **Gießen**, Germany
S. Bodenschatz, K.T. Brinkmann, V. Di Pietro, S. Diehl, V. Dormenev, M. Düren, E. Etzelmüller, K. Föhl, M. Galuska, T. Geßler, E. Gutz, C. Hahn, A. Hayrapetyan, M. Kesselkaul, W. Kühn, T. Kuske, J. S. Lange, Y. Liang, O. Merle, V. Metag, M. Moritz, M. Nanova, R. Novotny, T. Quagli, A. Riccardi, J. Rieke, M. Schmidt, R. Schnell, H. Stenzel, M. Strickert, U. Thöring, T. Wasem, B. Wohlfahrt, H.G. Zaunick

IRFU, CEA, Université Paris-Saclay, **Gif-sur-Yvette Cedex**, France
E. Tomasi-Gustafsson

University of Glasgow, **Glasgow**, United Kingdom
D. Ireland, G. Rosner, B. Seitz

Birla Institute of Technology and Science, Pilani, K K Birla Goa Campus, **Goa**, India
P.N. Deepak, A. Kulkarni

KVI-Center for Advanced Radiation Technology (CART), University of Groningen, **Groningen**, Netherlands
A. Apostolou, M. Babai, M. Kavatsyuk, H. Loehner, J. Messchendorp, P. Schakel, M. Tiemens, J. C. van der Weele, S. Vejdani

Gauhati University, Physics Department, **Guwahati**, India
K. Dutta, K. Kalita

Fachhochschule Südwestfalen, **Iserlohn**, Germany
H. Sohlbach

Forschungszentrum Jülich, Institut für Kernphysik, **Jülich**, Germany
M. Bai, L. Bianchi, M. Büscher, A. Derichs, R. Dosdall, A. Erven, V. Fracassi, A. Gillitzer, F. Goldenbaum, D. Grunwald, L. Jokhovets, G. Kemmerling, H. Kleines, A. Lai, A. Lehrach, M. Mikirtychyants, S. Orfanitski, D. Prasuhn, E. Prencipe, J. Pütz, J. Ritman, E. Rosenthal, S. Schadmand, T. Sefzick, V. Serdyuk, G. Sterzenbach, T. Stockmanns, P. Wintz, P. Wüstner, H. Xu, Y. Zhou

Chinese Academy of Science, Institute of Modern Physics, **Lanzhou**, China
Z. Li, X. Ma, H. Xu

INFN Laboratori Nazionali di Legnaro, **Legnaro**, Italy
V. Rigato

Lunds Universitet, Department of Physics, **Lund**, Sweden
L. Isaksson

Johannes Gutenberg-Universität, Institut für Kernphysik, **Mainz**, Germany
P. Achenbach, A. Aycock, O. Corell, A. Denig, M. Distler, M. Hoek, W. Lauth, Z. Liu, H. Merkel, U. Müller, J. Pochodzalla, S. Sanchez, S. Schlimme, C. Sfienti, M. Thiel, M. Zambrana

Helmholtz-Institut Mainz, **Mainz**, Germany
H. Ahmadi, S. Ahmed , S. Bleser, L. Capozza, M. Cardinali, A. Dbeyssi, A. Ehret, B. Fröhlich, P. Grasemann, S. Haasler, D. Izard, J. Jorge, D. Khaneft, R. Klasen, R. Kliemt, J. Köhler, H. H. Leithoff, D. Lin, F. Maas, S. Maldaner, M. Michel, M. C. Mora Espí, C. Morales Morales, C. Motzko, O. Noll, S. Pflüger, D. Rodríguez Piñeiro, M. Steinen, E. Walaa, S. Wolff, I. Zimmermann

Research Institute for Nuclear Problems, Belarus State University, **Minsk**, Belarus
A. Fedorov, M. Korzhik, O. Missevitch

Institute for Theoretical and Experimental Physics, **Moscow**, Russia
P. Balanutsa, V. Chernetsky, A. Demekhin, A. Dolgolenko, P. Fedorets, A. Gerasimov, V. Goryachev, D. Y. Kirin, V. A. Matveev, A. V. Stavinskiy

Moscow Power Engineering Institute, **Moscow**, Russia
A. Balashoff, A. Boukharov, O. Malyshev, I. Marishev

Nuclear Physics Division, Bhabha Atomic Research Centre, **Mumbai**, India
V. Chandratre, V. Datar, V. Jha, H. Kumawat, A.K. Mohanty, A. Parmar, A. K. Rai, B. Roy, G. Sonika

Westfälische Wilhelms-Universität Münster, **Münster**, Germany
C. Fritzsch, S. Grieser, A.K. Hergemöller, B. Hetz, N. Hüsken, A. Khoukaz, J. P. Wessels

Suranaree University of Technology, **Nakhon Ratchasima**, Thailand
C. Herold, K. Khosonthongkee, C. Kobdaj, A. Limphirat, P. Srisawad, Y. Yan

Novosibirsk State University, **Novosibirsk**, Russia
A. E. Blinov, S. Kononov, E. A. Kravchenko

Budker Institute of Nuclear Physics, **Novosibirsk**, Russia
E. Antokhin, M. Barnyakov, A. Yu. Barnyakov, K. Beloborodov, V. E. Blinov, V. S. Bobrovnikov, I. A. Kuyanov, A. P. Onuchin, S. Pivovarov, E. Pyata, S. Serednyakov, Y. Tikhonov

Institut de Physique Nucléaire, CNRS-IN2P3, Univ. Paris-Sud, Université Paris-Saclay, 91406, **Orsay cedex**, France
R. Kunne, D. Marchand, B. Ramstein, J. van de Wiele, Y. Wang

Dipartimento di Fisica, Università di Pavia, INFN Sezione di Pavia, **Pavia**, Italy
G. Boca

Charles University, Faculty of Mathematics and Physics, **Prague**, Czech Republic
V. Burian, M. Finger, M. Finger, A. Nikolovova, M. Pesek, M. Peskova, M. Pfeffer, I. Prochazka, M. Slunecka

Czech Technical University, Faculty of Nuclear Sciences and Physical Engineering, **Prague**, Czech Republic
P. Gallus, V. Jary, J. Novy, M. Tomasek, M. Virius, V. Vrba

Institute for High Energy Physics, **Protvino**, Russia
V. Abramov, N. Belikov, S. Bukreeva, A. Davidenko, A. Derevschikov, Y. Goncharenko, V. Grishin, V. Kachanov, V. Kormilitsin, A. Levin, Y. Melnik, N. Minaev, V. Mochalov, D. Morozov, L. Nogach, S. Poslavskiy, A. Ryazantsev, S. Ryzhikov, P. Semenov, I. Shein, A. Uzunian, A. Vasiliev, A. Yakutin

Sikaha-Bhavana, Visva-Bharati, WB, **Santiniketan**, India
U. Roy

University of Sidney, School of Physics, **Sidney**, Australia
B. Yabsley

National Research Centre "Kurchatov Institute" B. P. Konstantinov Petersburg Nuclear Physics Institute, Gatchina, **St. Petersburg**, Russia
S. Belostotski, G. Gavrilov, A. Izotov, S. Manaenkov, O. Miklukho, D. Veretennikov, A. Zhdanov

Kungliga Tekniska Högskolan, **Stockholm**, Sweden
T. Bäck, B. Cederwall

Stockholms Universitet, **Stockholm**, Sweden

K. Makonyi, M. Preston, P.E. Tegner, D. Wölbing

Veer Narmad South Gujarat University, Department of Physics, **Surat**, India
S. Godre

Università di Torino and INFN Sezione di Torino, **Torino**, Italy
M. P. Bussa, S. Marcello, S. Spataro

Politecnico di Torino and INFN Sezione di Torino, **Torino**, Italy
F. Iazzi, R. Introzzi, A. Lavagno

INFN Sezione di Torino, **Torino**, Italy
D. Calvo, P. De Remigis, A. Filippi, G. Mazza, A. Rivetti, R. Wheadon

Università di Trieste and INFN Sezione di Trieste, **Trieste**, Italy
A. Martin

Uppsala Universitet, Institutionen för fysik och astronomi, **Uppsala**, Sweden
H. Calen, W. Ikegami Andersson, T. Johansson, A. Kupsc, P. Marciniewski, M. Papenbrock, J. Pettersson, J. Regina, K. Schönning, M. Wolke

Instituto de Física Corpuscular, Universidad de Valencia-CSIC, **Valencia**, Spain
J. Diaz

Sardar Patel University, Physics Department, **Vallabh Vidynagar**, India
V. Pothodi Chackara

National Centre for Nuclear Research, **Warsaw**, Poland
A. Chlopik, G. Kesik, D. Melnychuk, B. Slowinski, A. Trzcinski, M. Wojciechowski, S. Wronka, B. Zwieglinski

Österreichische Akademie der Wissenschaften, Stefan Meyer Institut für Subatomare Physik, **Wien**, Austria
P. Bühler, J. Marton, D. Steinschaden, K. Suzuki, E. Widmann, S. Zimmermann, J. Zmeskal

---

Editors:

Michael Düren	Email: michael.dueren@exp2.physik.uni-giessen.de
Erik Etzelmüller	Email: erik.etzelmueller@exp2.physik.uni-giessen.de
Klaus Föhl	Email: klaus.foehl@exp2.physik.uni-giessen.de
Avetik Hayrapetyan	Email: avetik.hayrapetyan@exp2.physik.uni-giessen.de
Matthias Hoek	Email: hoek@uni-mainz.de
Albert Lehmann	Email: albert.lehmann@physik.uni-erlangen.de
Julian Rieke	Email: julian.rieke@physik.uni-giessen.de
Mustafa Schmidt	Email: mustafa.schmidt@exp2.physik.uni-giessen.de

Technical Coordinator:

Lars Schmitt	Email: l.schmitt@gsi.de

Spokesperson:

Klaus Peters	Email: k.peters@gsi.de

Deputy:

Tord Johansson	Email: tord.johansson@physics.uu.se

Preface

PANDA (anti-Proton ANnihiliation at DArmstadt) is planned to be one of the four main experiments at the future international accelerator complex FAIR (Facility for Antiproton and Ion Research) in Darmstadt, Germany. It is going to address fundamental questions of hadron physics and quantum chromodynamics using cooled antiproton beams with a high intensity and and momenta between 1.5 and 15 GeV/c. PANDA is designed to reach a maximum luminosity of $2 \times 10^{32}\,\mathrm{cm}^{-2}\,\mathrm{s}$. Most of the physics programs require an excellent particle identification (PID). The PID of hadronic states at the forward endcap of the target spectrometer will be done by a fast and compact Cherenkov detector that uses the detection of internally reflected Cherenkov light (DIRC) principle. It is designed to cover the polar angle range from 5° to 22° and to provide a separation power for the separation of charged pions and kaons up to 3 standard deviations (s.d.) for particle momenta up to 4 GeV/c in order to cover the important particle phase space. This document describes the technical design and the expected performance of the novel PANDA Disc DIRC detector that has not been used in any other high energy physics experiment (HEP) before. The performance has been studied with Monte-Carlo simulations and various beam tests at DESY and CERN. The final design meets all PANDA requirements and guarantees sufficient safety margins.

Contents

Preface **vii**

1 Executive Summary **1**

2 The $\overline{\text{P}}$ANDA Experiment and its PID Concept **5**

2.1 The $\overline{\text{P}}$ANDA Experiment 5
2.1.1 The Scientific Program 5
2.1.2 High Energy Storage Ring 5
2.1.3 Targets 6
2.1.4 Luminosity Considerations 6
2.2 The $\overline{\text{P}}$ANDA Detector 6
2.2.1 Target Spectrometer 7
2.2.2 Forward Spectrometer 7
2.2.3 Data Acquisition 8
2.2.4 Infrastructure 8
2.3 The Particle Identification System . . 8
2.3.1 Tracking Detectors 8
2.3.2 EM Calorimeter 8
2.3.3 Cherenkov Detectors 9
2.3.4 Time-Of-Flight Detectors 10
2.3.5 Muon Detection 10
2.3.6 Combined PID 10

3 Design of the Disc DIRC **11**

3.1 Overview 11
3.2 Goals and Requirements 12
3.3 Detector Design 13

4 Detector Components **17**

4.1 Optical Components 17
4.1.1 Radiator 17
4.1.2 Imaging Optics 20
4.1.3 Optical Joints 24
4.2 Photon Sensors 24
4.2.1 Requirements 24
4.2.2 Photon Sensor Options 27
4.2.3 Evaluation of MCP-PMTs 27
4.2.4 Conclusions 41
4.3 Frontend Electronics 41
4.3.1 Requirements 41
4.3.2 Fast Digitization 41
4.3.3 Data Concentration and Computing 44
4.4 Detector Control, Monitoring and Calibration 44
4.4.1 Detector Control System 44
4.4.2 Laser Monitoring System 45
4.4.3 Optical Calibration and Alignment 46
4.4.4 In-beam Calibration and Alignment 46

5 Performance of the Detector System **49**

5.1 Prototype Tests 49
5.1.1 A fast Cherenkov Counter Prototype using dSiPMs in 2010 49
5.1.2 Measurement of DIRC Cherenkov Patterns at DESY in 2011 and 2012 49
5.1.3 Particle Identification with a DIRC Prototype at CERN in 2012 51
5.1.4 Prototype Test with MCP-PMT Sensors at CERN in 2015 53
5.1.5 Prototype Test with TOFPET Readout at DESY 2016 56
5.2 Final Endcap Disc DIRC 62
5.2.1 Expected Detector Performance . 62
5.2.2 PID Performance using Two Different Analysis Methods 63
5.2.3 Overall Performance using two different Photocathode Options . 66
5.3 Conclusions 68

6 Mechanics and Integration **71**

6.1 Design Approach 71
6.2 Integration into $\overline{\text{P}}$ANDA 74
6.2.1 Neighboring Subdetectors 74
6.2.2 Assembly Procedure 74
6.3 Supply Lines and Cables 77
6.4 Maintenance 78

7 Project Management **81**

7.1 Work packages 81

7.2 Schedule 81
7.3 Manpower 81
7.4 Quality Control 83
7.4.1 Optical Elements 83
7.4.2 Sensors and Readout 83
7.4.3 The Quadrant 83
7.4.4 System Integration 83
7.5 Safety 84
7.5.1 Mechanics 84
7.5.2 Electrical Equipment and Cooling 84
7.5.3 Radiation Aspects 84

8 Acknowledgements **84**

List of Acronyms **86**

1 Executive Summary

The $\overline{\text{P}}$ANDA Experiment

$\overline{\text{P}}$ANDA [1] will be one of the main experiments for the new international accelerator complex FAIR (Facility for Antiproton and Ion Research) in Darmstadt, Germany. A stored and cooled antiproton beam of 1.5 - 15 GeV/c momentum, colliding with a fixed proton or nuclear target, will allow for high luminosity hadron production and formation experiments. The annihilating baryons will produce new particles at high rate and with various quantum numbers, giving insight into the properties of mesons and baryons and the strong interactions of quarks and gluons. Recently discovered new hadronic states, especially the Z^+ (4430) [2], which is most likely an exotic state, will be mapped out in detail and searches for other exotic matter, especially glueballs, will be performed.

To cope with high production rates and complex hadronic final states, a 4π detector is designed with excellent tracking, calorimetry, and particle identification. It will be read out in a triggerless mode. The importance of the charm quark sector for the study of exotic states requires the use of the $\overline{\text{P}}$ANDA electromagnetic calorimeter for photon detection, the micro vertex detector for the measurement of sub-mm decay lengths, and the positive identification of charged kaons.

The identification of charged particles is implemented in three angular regions: The region of the barrel EMC (polar angles 22° - 140°) will be equipped with a Barrel DIRC (where DIRC stands for Detection of Internally Reflected Cherenkov light) [3]; the endcap EMC region (5° - 22°) with the Endcap Disc DIRC (EDD) described here, and the very forward region (< 5°) with an aerogel RICH detector downstream of the forward spectrometer. In addition time-of-flight counters are provided for low momentum particle identification. Muons will be identified by a dedicated muon detection system which also serves as a hadronic calorimeter.

A compact, fast Disc DIRC

This document describes the proposed EDD for $\overline{\text{P}}$ANDA. The requirement is to positively identify kaons in the momentum range of 1 - 4 GeV/c, i.e. to separate kaons from pions and protons. Muons are identified in muon chambers.

DIRC detectors make use of internally reflected Cherenkov light in a solid state radiator. Here a transparent fused silica plate of 20 mm thickness is employed. The photons are read out at the rim of the plate. This design makes DIRC detectors very thin, usually just a few centimeters, whereas other RICH detectors typically occupy an order of magnitude more space along the path of the detected particles. The EDD is significantly more economic than a RICH design as the forward endcap EMC and the complete forward spectrometer can be moved closer to the interaction point. Therefore, the transverse size of the subsequent detectors can be reduced.

More than 10 years of R&D have been invested into the current, novel design of a Disc DIRC. Several versions have been investigated in order to minimize cost and to maximize performance. The EDD will be the first Disc DIRC in a physics experiment. The $\overline{\text{P}}$ANDA requirements of the EDD are at the limit of today's technology. A major challenge is the readout of individual Cherenkov photons with high detection efficiency and at high rates in an environment with large background, high radiation dose, tight spatial constraints, and a large magnetic field. Only recently the technology of microchannel-plate photomultipliers (MCP-PMTs) has advanced such that the proposed EDD becomes feasible.

The EDD design uses a very limited number of component types, has a modular structure, a rigid optical setup, and can be fabricated by external companies to a large extend. This way, we aim to achieve a stable and reliable operation even with a limited manpower during construction, operation, and maintenance. The EDD consists of four identical quadrants, each of them is a fully functional PID detector that is mechanically, optically, and electronically separated from the other quadrants. A common holding cross aligns the quadrants mechanically. It is mounted on the holding structure of the forward endcap EMC.

The Quadrant

Each quadrant consists of a radiation hard, precision polished synthetic fused silica plate that forms the active area of the detector. Charged particles that traverse the radiator produce Cherenkov light. About half of the Cherenkov photons undergo multiple total reflections off the surfaces until they leave the plate at the outer rim. Attached to the rim

are light guide bars and focusing elements (FELs) which guide and focus the photons onto position-sensitive MCP-PMTs. The position registered by the photon sensor in the focal area of the FEL is used to extract the Cherenkov angle and, thus, the velocity of the particle that traverses the radiator. The precise timing of the MCP-PMT signal relative to the timing of other photons is used to separate the signal from background and to disentangle the photon pattern with different numbers of reflections at the rim of the radiator plate.

The radiator plate is an irregular hexagon and has three outer edges which are equipped with eight optical readout modules (ROMs) each. A ROM consists of an MCP-PMT, three FELs, and three connecting light guide bars. The radiator, the light guide bar, and the focusing element are optically bonded with high precision and form a rigid mechanical unit.

The Readout Module

Each of the 96 ROMs of the EDD is a separate readout unit. The MCP-PMT which is attached to each ROM has an anode structure with at least 3×100 pixels. The pixels with a pitch of not more than 0.5 mm measure the Cherenkov angle. The three columns are assigned to the three light guide bars and constitute the azimuthal resolution of the EDD. Each MCP-PMT anode surface is attached to a small PCB that holds several ASICs (Application Specific Integrated Circuits) which discriminate and digitize the analog MCP-PMT signals. A front-end board contains the low voltage control and concentrates the data from the ASICs onto an optical fiber link which brings the signals out of the experimental area to the $\overline{\text{P}}$ANDA DAQ system.

Major Components

The detector consists of 4 identical rigid optical units (radiator and FELs) in a common rigid mechanical frame and 96 identical opto-electronic readout modules calles ROMs (consisting of three FELs, MCP-PMT with front-end electronics, and an optical fibre). The specifications of the elements present a challenge. The critical items are the optical elements, the MCP-PMTs, and the readout electronics.

The optical elements will be manufactured by suitable optical companies according to the specifications. The assembly and the quality control will partly be done by the Cherenkov group in dedicated optical labs and by companies.

Until recently, MCP-PMTs had a very limited lifetime due to degradation effects of the photocathode after large exposure. New developments by several companies solved the lifetime problem to the extent that today's MCP-PMTs can stand integrated anode currents of more than $15\,\mathrm{C}/cm^2$ [4]. In our design the integrated charge will be limited by adding an optical band or long-pass filter in front of the MCP-PMTs to reduce the incident photon rate. Current developments also provide an option where the sensitivity of the MCP-PMT photocathodes is shifted towards higher wavelengths. The drawback of the reduced photon statistics is partially compensated by a reduction of the dispersion effects on the photon patterns. Currently, three companies are developing MCP-PMTs with the required spatial resolution. First prototypes have been developed and are currently being evaluated.

The heart of the front-end electronics is a modified version of the TOFPET ASIC [5]. This commercially available ASIC is suitable for our application concerning charge sensitivity, rate, and time resolution. In a common effort of several $\overline{\text{P}}$ANDA groups the chip is modified for $\overline{\text{P}}$ANDA applications. The same chip is planned to be used for the Barrel Time-of-Flight detector[6] and a similar version of the chip is planned for the MVD[7]. In all cases the digital part of the chip needs modifications which are currently being designed and tested.

Performance

Different versions of the EDD have been studied in detailed simulations and a sophisticated pattern reconstruction program has been developed where the particle type can be determined from time-ordered photon signals of the MCP-PMT anodes using likelihood methods. All known effects of the optical transmission including focusing, scattering, absorption, quantum efficiencies of the photocathode, and degradation of the surfaces are included in the simulation. Minimum bias events at full $\overline{\text{P}}$ANDA luminosity and dark count rates of the MCP-PMTs have been included. The optimized version of the EDD shows a performance that meets the requirements of $\overline{\text{P}}$ANDA. The design will deliver the required separation power between pions and kaons in most of the phase space for momenta up to 4 GeV/c.

Lab and Beam Tests

The individual optical and electronic components of the EDD have been tested intensively in the lab. Small-scale prototypes have been evaluated success-

fully in test beam experiments. At mixed hadron beams at CERN the capabilities of the EDD have been demonstrated by providing a clean separation for pions and protons at 3 GeV/c on a single photon level. Furthermore, it was shown that the measured single photon resolutions and the number of detected Cherenkov photons agree with Monte Carlo simulations.

References

[1] PANDA Collaboration. Physics Performance Report for PANDA: Strong Interaction Studies with Antiprotons. 2009.

[2] S.-K. Choi et al. Observation of a Resonance-like Structure in the $\pi^{+-}\psi'$ Mass Distribution in exclusive $B \to k\pi^{+-}\psi'$ Decays. *Phys. Rev. Lett.*, 100:142001, 2008.

[3] B. Singh et al. Technical design report for the PANDA Barrel DIRC detector. *Journal of Physics G: Nuclear and Particle Physics*, 46(4):045001, mar 2019.

[4] A. Lehmann et al. Lifetime of MCP-PMTs. *J. Instrum.*, 11:C05009, 2016.

[5] M.D. Rolo et al. TOFPET ASIC for PET applications. *J. Instrum.*, 8:C02050, 2013.

[6] B. Singh and others (PANDA Collaboration). Technical Design Report for the PANDA Barrel Time-of-Flight. *Internal Report FAIR, Darmstadt, https://fair-center.eu/en/for-users/publications/*, 2018.

[7] PANDA Collaboration. Technical Design Report for the: PANDA Micro Vertex Detector. arXiv:1207.6581, 2011.

2 The $\overline{\text{P}}$ANDA Experiment and its PID Concept

2.1 The $\overline{\text{P}}$ANDA Experiment

2.1.1 The Scientific Program

The $\overline{\text{P}}$ANDA (anti-Proton ANnihiliation at DArmstadt) collaboration [1] envisages a physics core program [2] that comprises

- charmonium spectroscopy with precision measurements of mass, width and decay branches;
- the investigation of states that are assumed to have more exotic configurations like multiquark states, charmed hybrids and glueballs;
- the search for medium modifications of charmed hadrons in nuclear matter;
- the γ-ray spectroscopy of hypernuclei, in particular double-Λ states.

In charmonium spectroscopy, for example, theoretical calculations differ significantly above the $D\bar{D}$ threshold and do not properly predict several recently discovered states. Experimentally, a fair number of states and their properties at higher energy are not well established.

Charmonia states have been observed in e^+e^- interactions as well, where only 1^{--} states are directly formed, which limits the number of resonances that can be accurately scanned by ramping the accelerator energy. In $\bar{p}p$ reactions more meson states can be directly formed, and an excellent mass resolution of $\sigma = 20\,\text{keV}$ allows an accurate determination of the width of a resonance.

Further states (spin exotics) can be studied using the production mechanism.

2.1.2 High Energy Storage Ring

The combination of the High Energy Storage Ring (HESR) and $\overline{\text{P}}$ANDA aims at both high reaction rates and high resolution to be able to study rare production processes and small branching ratios. With up to 10^{11} stored antiprotons for beam momenta from 1.5 to 15 GeV/c and high density targets the anticipated antiproton production rate of $2{\cdot}10^7\,\text{s}^{-1}$ governs the experiment interaction rate

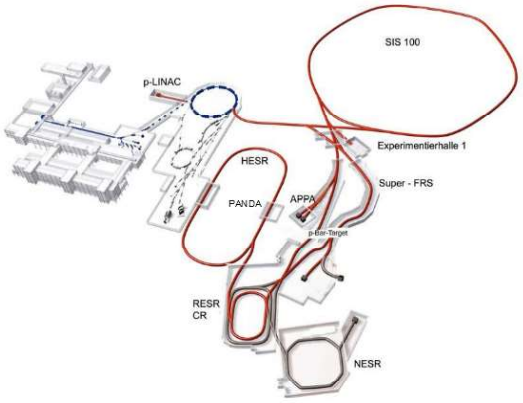

Figure 2.1: Schematic of the future FAIR layout incorporating the current GSI installations on the left; on the right the future installations, among them the SIS 100 synchrotron, the storage and cooler ring complex including CR and HESR, and the Super FRS experiments (reproduced from [3]).

in the order of cycle-averaged $1{\cdot}10^7\,\text{s}^{-1}$. The stored antiprotons do not have a bunch structure, and with 10–20% allocated to a barrier bucket, the antiprotons are continuously spread over 90–80% of the HESR circumference.

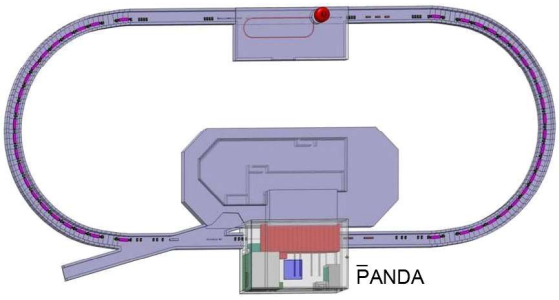

Figure 2.2: The HESR ring with the $\overline{\text{P}}$ANDA experimental area at the bottom (marked in red) and the electron cooler installation at the top. Standard operation has the antiproton injection from RESR (during the modularized startup phase from CR) from the left. Protons may be incected at reversed field polarities.

Two complementary operating modes are planned, named *high luminosity* and *high resolution*. The high luminosity mode with a momentum resolution of $\Delta p/p = 10^{-4}$, stochastic cooling and a pellet target density of $4 \cdot 10^{15}\,\text{cm}^{-2}$ will have a luminosity of

$L = 2 \cdot 10^{32}\,\mathrm{cm^{-2}s^{-1}}$. For the high resolution mode $\Delta p/p = 4 \cdot 10^{-5}$ will be achieved with electron cooling for momenta up to $p = 8.9\,\mathrm{GeV/c}$. This mode will operate in conjunction with a cluster jet target to limit the energy broadening caused by the target. The cycle-averaged luminosity is expected to be $L = 1 \cdot 10^{31}\,\mathrm{cm^{-2}s^{-1}}$.

2.1.3 Targets

The PANDA Target Spectrometer is designed to allow the installation of different targets [1, 4]. For hydrogen as target material both Cluster Jet and Pellet Targets are being prepared. A major technical challenge is the distance of 2.5 m between the target generation and the accelerator beam and the distance of 5 m between the target generation and the target dump.

The cluster jet should give a constant thickness as a function of time whereas a pellet beam with its granular structure may give density variations on the $10 - 100\,\mu$s timescale. The cluster jet gives a larger interaction region and is anticipated to cause more background gas than the pellets for similar target thickness, the latter according to results from comparative studies made at CELSIUS and at COSY.

An extension of the targets to heavier gases such as deuterium, nitrogen or argon is planned for complementary studies with nuclear targets.

2.1.4 Luminosity Considerations

The luminosity is proportional to the number of stored antiprotons and is limited by the antiproton production rate. To first approximation the cycle averaged reaction rate should equal the antiproton production rate. Due to injection time and dumping of beam particles at the end of a cycle the time averaged reaction rate will be lower. Figure 2.3 illustrates beam preparation periods with target off and data taking periods with target on. The red curve shows the luminosity at constant target thickness which is proportional to the decreasing number of antiprotons during data taking. Measures to implement a target density increasing with time are studied in order to achieve constant luminosity.

Some variations of the instantaneous luminosity on short time scales of milliseconds and below will occur due to the target. The newly developed PANDA cluster jet target is expected to give small variations. In the case of a pellet target, variations of the instantaneous luminosity may occur. These are

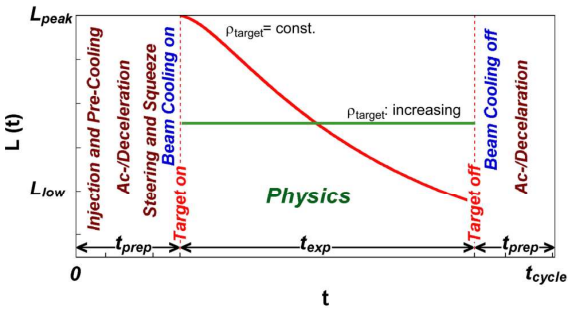

Figure 2.3: Time dependent macroscopic luminosity profile $L(t)$ in one operation cycle for constant (solid red) and increasing (green dotted) target density ρ_{target} [5]. Different measures for beam preparation are indicated. Pre-cooling is performed at 3.8 GeV/c. A maximum ramp of 25 mT/s is specified for beam ac-/deceleration.

depending on antiproton beam profile, pellet size and distributions of pellet velocity and spacing between pellets.

The design goal of the pellet target in high luminosity (PHL) mode is to always have more than 10 small pellets (with diameters ¡ 10 μm) in the beam region. In this mode, the velocity spread is not very crucial and one could have a stochastic time distribution of pellets. This would cause luminosity variations below 30% [4].

In pellet tracking (PTR) mode the pellet velocity spread should be below the per cent level for highly effective tracking. In this mode there will most of the time be only one pellet in the interaction region and its position will be known with high accuracy. At the pellet tracking development station (UPTS), the velocity spread is a few per mille and for this case only occasionally there would be two or more pellets in the beam region [4].

Target density fluctuations and background level will be taken into account when optimizing target settings in order to avoid that the maximum total interaction rate will exceed the 10 MHz mark.

2.2 The $\overline{\text{P}}$ANDA Detector

Figure 2.4 shows the $\overline{\text{P}}$ANDA detector as a partial cut-out. $\overline{\text{P}}$ANDA is a fixed target experiment and consists of two parts, the Target Spectrometer and the Forward Spectrometer. The antiproton beam is scattered off a pellet or cluster jet target. $\overline{\text{P}}$ANDA will be measuring $\mathrm{p\bar{p}}$ reactions comprehensively and exclusively, which requires simultaneous measurements of leptons and photons as well as charged

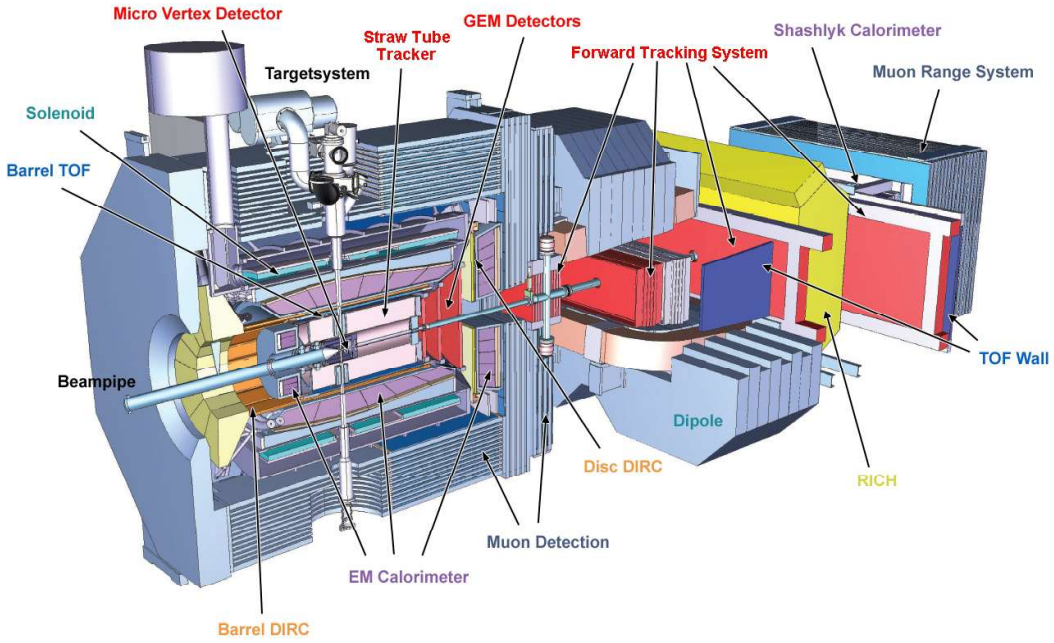

Figure 2.4: Side view of $\overline{P}$ANDA with the target spectrometer (TS) on the left side, and the forward spectrometer (FS) starting with the Dipole magnet center and right. The antiproton beam enters from the left.

and neutral hadrons, with high multiplicities.

The physics requirements for the detectors are:

- cover the full solid angle of the released particles,
- detect the momenta of the charged reaction products,
- measure the energy of photons,
- measure decay vertices of strange and charm particles,
- identify particle types over the full range of momenta of the reaction products.

2.2.1 Target Spectrometer

The Target Spectrometer components, subdivided into backward endcap, barrel and forward endcap regions, are housed within the yoke of a superconducting solenoid magnet [6]. The Target Spectrometer is almost hermetically sealed to avoid solid angle gaps and provides little spare space inside. Parts of the return yoke iron are laminated to allow the insertion of muon detectors into the gaps. Most components are located inside the magnetic field of the solenoid magnet.

The silicon microvertex detector (MVD) [7] closely abuts the beam pipe surrounding the target area. It provides secondary vertex sensitivity for particles with decay lengths on the order of 100 μm.

The central tracker features the straw tube tracker and several GEM tracking stations in the forward endcap part [5].

Two detectors of internally reflected Cherenkov light (DIRC) are to be located with the target spectrometer. The possibility of using thin radiators and placing the readout elements outside the acceptance favors the use of DIRC designs as Cherenkov imaging detectors for PID.

The lead tungstate (PWO) crystals of the electromagnetic calorimeters (EMC) [8] are read out with avalanche photo diodes (APD) or vacuum pentodes. Both, the crystal light output and the APD performance improve with lower temperature. Thus, plan is to operate the EMC at T = –25°C.

2.2.2 Forward Spectrometer

The Forward Spectrometer angular acceptance has an ellipsoidal form with a maximum polar angle of ±10 degrees horizontally and ±5 degrees vertically.

A dipole magnet is located at the most upstream part of the Forward Spectrometer to provide bending power with a vertical B-field. The majority of the detector systems (the exception being tracking sensors) are located downstream and outside the

dipole magnet.

An aerogel RICH detector will be located between the dipole magnet and the Forward EMC. A Time-of-Flight wall covers slow particles below the Cherenkov light threshold.

In the Forward Spectrometer, a Shashlyk type electromagnetic calorimeter (scintillator fibers in a lead matrix) is followed by a scintillator-absorber-sandwich hadron calorimeter.

2.2.3 Data Acquisition

The data flow and processing is geometrically separated into the front-end electronics (FEE) located with the actual detector subsystems and comprises analog electronics, digitization, and (depending on subsystem) a first data concentrator stage.

After data transmission via optical fiber links the data acquisition (DAQ) is located in the Counting House, where the online analysis and data concentration (a factor 1000 according to the current paradigm) is handled before the data is sent to storage.

The overall data acquisition setup will have to cope with peak rates above the mean data rate of $\sim 200\,\text{GB/s}$. Bursts on different timescales are due to antiproton beam time structure, target density fluctuations (in case of pellet target) and luminosity decrease during the HESR operation cycle.

2.2.4 Infrastructure

The $\overline{\text{P}}$ANDA detector is located underground in an experimental hall, encased in smaller tunnel-like concrete structures, partially fixed, partially made of removable blocks. Most subsystems connect their FEE-components via cables and tubes placed in movable cable ducts to the installations in the counting house, where three levels are planned to accommodate cooling, gas supplies, power supplies and electronics. Electronic racks for only a few subcomponents will be placed directly next to the Target Spectrometer.

The EDD's FEE and digitization will be located inside the solenoid yoke of the target spectrometer. Cooling, low and high voltage, a nitrogen flow system and a laser calibration system will be supplied from the counting house.

2.3 The Particle Identification System

The charged particle identification (PID) will combine time-of-flight, tracking, dE/dx and calorimetry information with the output from imaging Cherenkov detectors.

The individual $\overline{\text{P}}$ANDA subsystems contributing to the PID and the combination into global PID information have been reviewed in the PID-TAG-report [9]. The contents relevant for this EDD-TDR is included below.

2.3.1 Tracking Detectors

Tracking information provides input to the DIRC analysis, as the Cherenkov angle is measured between the Cherenkov photon direction and the vertex of the radiating particle.

Tracking Detectors like the MVD and STT also provide information as the mean energy loss of charged particles per unit length depends on the velocity rather than the momentum. It is usually referred to as dE/dx and is described by the Bethe Bloch equation which depends on the velocity rather than the momentum of the charged particle. The dE/dx contributes to low energy PID at typically $p < 1\,\text{GeV/c}$ (see Figure 2.5).

Several GEM detector stations of the $\overline{\text{P}}$ANDA Target Spectrometer provide tracking information for the forward and endcap polar angles. The tracking information with an accuray of $\sigma \approx 1\,\text{mrad}$ enters into the analysis of the EDD.

2.3.2 EM Calorimeter

In the $\overline{\text{P}}$ANDA Target Spectrometer high precision electromagnetic calorimetry is required for a large energy range from a few MeV up to several GeV [8]. Lead-tungstate is chosen for the calorimeters in the target spectrometer due to its good energy resolution, fast response and high density, allowing a compact setup.

In addition to photon detection, the EMC is also the most powerful detector for the identification of electrons. The identification and measurement of this particle species will play an essential role for the physics program of $\overline{\text{P}}$ANDA.

The stopping power of an electromagnetic calorimeter is different for electrons, muons and hadrons. While muons and hadrons loose only a certain fraction of their kinetic energy by ionization processes,

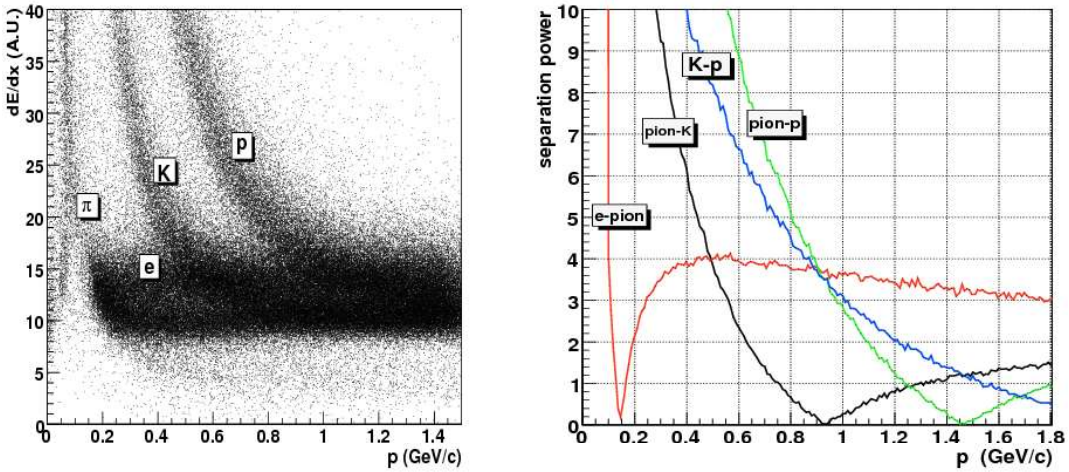

Figure 2.5: Energy loss by a 40% truncated mean algorithm for various particles versus the reconstructed momentum (left) and corresponding separation power (right) in the STT detector [9].

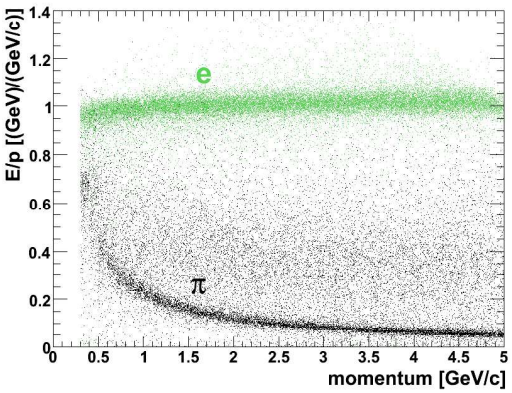

Figure 2.6: Simulated E/p versus track momentum for electrons (green) and pions (black) in the momentum range between 0.3 GeV/c and 5 GeV/c typical for Barrel and Endcap EMC [8, 9].

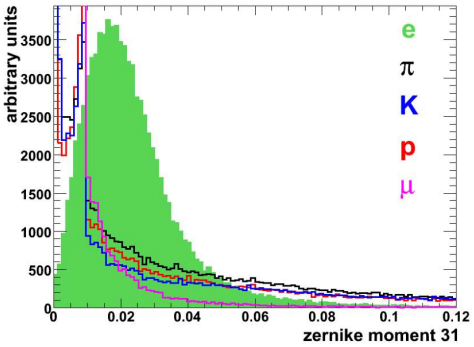

Figure 2.7: Zernike moment z31 for electrons, muons and hadrons [8].

electrons deposit their complete energy in an electromagnetic shower. The ratio of the measured energy deposit in the calorimeter to the reconstructed track momentum (E/p) will be approximately one. Due to the fact that hadronic interactions within the crystals can take place, hadrons can have a higher E/p ratio than expected from ionization. Figure 2.6 shows the reconstructed E/p fraction for electrons and pions as a function of momentum.

Furthermore, the shower shape of a cluster is helpful to distinguish between electrons, muons and hadrons. Since the size of the crystals corresponds to the Molière radius of lead tungstate, the largest fraction of an electromagnetic shower originating from an electron is contained in a few crystals. A hadronic shower with a similar energy deposit has smaller lateral extension. The differences are reflected in the shower shape of the cluster, which can be characterized by single crystal to sum energy ratio, the lateral cluster moment and Zernike moments. Figure 2.7 shows the different distributions for the Zernike moment z31.

The crystal calorimeters of the Target Spectrometer are complemented in the forward direction with the shashlik type sampling calorimeter of the Forward Spectrometer consisting of 1404 modules of 55×55 mm^2 cell size covering 2.97×1.43 m^2.

2.3.3 Cherenkov Detectors

The endcap part of the Target Spectrometer covers forward angles up to $\vartheta = 22°$, excluding an inner elliptical acceptance of $\vartheta_x = 10°$ horizontal and $\vartheta_y = 5°$ vertical half-angles. The Endcap Disc DIRC (EDD) is will be located here.

A second DIRC, the Barrel DIRC covers the angular range from $\vartheta = 22°$ to 140°. The design [10] is based on the DIRC of the BaBar experiment [11].

An aerogel RICH detector will be located between the dipole magnet and the Forward EMC. Its design can be similar to the RICH detector in HERMES at DESY [12], possibly using four curved mirrors instead of two or a pure proximity focusing design using flat mirrors.

2.3.4 Time-Of-Flight Detectors

In the Forward Spectrometer a time-of-flight (TOF) measurement is planned that covers slow particles below the Cherenkov light threshold. For the target spectrometer, a scintillator based TOF system with a SiPM readout is foreseen.

2.3.5 Muon Detection

The return yoke for the solenoid magnet in the $\overline{\text{P}}$ANDA Target Spectrometer is laminated to accommodate layers of muon detectors. They form a range stack, with the inner muon layer being able to detect low energy muons. The cumulated iron layer thickness in front of the outer layers provide sufficient material to stop the high energy pions produced in $\overline{\text{P}}$ANDA.

2.3.6 Combined PID

The particle identification (PID) capability of several subsystem combinations (different tracker designs, with or without TOF, etc.) has been studied in the PID-TAG working group. The combined PID performance for particle pairs of (e, μ, π, K, p) were presented in [9].

References

[1] PANDA Collaboration. Technical Progress Report. 2005.

[2] PANDA Collaboration. Physics Performance Report for PANDA: Strong Interaction Studies with Antiprotons. 2009.

[3] Peter Spiller, Frank Becker, Oleksiy Dolinskyy, Lars Groening, Oliver Kester, Klaus Knie, Dieter Prasuhn, Hartmut Reich-Sprenger, Wolfgang Vinzenz, and Martin Winkler. The Accelerator Facility of the Facility for Antiproton and Ion Research. In *Proceedings, 6th International Particle Accelerator Conference (IPAC 2015): Richmond, Virginia, USA, May 3-8, 2015*, page TUBB2, 2015.

[4] PANDA Collaboration. Technical Design Report for the PANDA Internal Targets. 2012.

[5] PANDA Collaboration. Technical Design Report for the: PANDA Straw Tube Tracker. arXiv:1205.5441, 2012.

[6] PANDA Collaboration. Technical Design Report for the PANDA Solenoid and Dipole Spectrometer Magnets. arXiv:0907.0169, 2009.

[7] PANDA Collaboration. Technical Design Report for the: PANDA Micro Vertex Detector. arXiv:1207.6581, 2011.

[8] PANDA Collaboration. Technical Design Report for: PANDA Electromagnetic Calorimeter (EMC). arXiv:0810.1216, 2008.

[9] G. Schepers et al. Particle Identification at PANDA. *Report of the PID TAG*, March 2009.

[10] B. Singh et al. Technical design report for the PANDA Barrel DIRC detector. *Journal of Physics G: Nuclear and Particle Physics*, 46(4):045001, mar 2019.

[11] I. Adam et al. The dirc particle identification system for the babar experiment. *Nuclear Instruments and Methods in Physics Research Section A: Accelerators, Spectrometers, Detectors and Associated Equipment*, 538(1):281 – 357, 2005.

[12] N. Akopov et al. The HERMES dual-radiator ring imaging Cherenkov detector. *Nucl. Instr. Meth. A*, 479:511–530, 2002.